AGU PUBLICATIONS

JGR

Journal of Geophysical Research: Oceans

RESEARCH ARTICLE

10.1002/2015JC011440

Horizontal mixing in the Southern Ocean from Argo float trajectories

Christopher J. Roach[1], Dhruv Balwada[2], and Kevin Speer[2,3]

[1]International Pacific Research Center, University of Hawaii, Honolulu, Hawaii, USA, [2]Geophysical Fluid Dynamics Institute, Contribution Number 477, Florida State University, Tallahassee, Florida, USA, [3]Department of Earth, Ocean and Atmospheric Science, Florida State University, Tallahassee, Florida, USA

Key Points:
- We show that Southern Ocean Argo float trajectories can provide circumpolar lateral diffusivity estimates
- Argo floats are used to quantify the variation of eddy diffusivity in the ACC showing enhancement in regions near topographic features
- Theory incorporating suppression by mean flow shows general similarity but does not accurately represent the enhanced regional values

Correspondence to:
C. Roach,
croach@hawaii.edu

Citation:
Roach, C. J., D. Balwada, and K. Speer (2016), Horizontal mixing in the Southern Ocean from Argo float trajectories, *J. Geophys. Res. Oceans*, *121*, 5570–5586, doi:10.1002/2015JC011440.

Received 4 NOV 2015
Accepted 22 JUN 2016
Accepted article online 27 JUN 2016
Published online 6 AUG 2016

Abstract We provide the first observational estimate of the circumpolar distribution of cross-stream eddy diffusivity at 1000 m in the Southern Ocean using Argo float trajectories. We show that Argo float trajectories, from the float surfacing positions, can be used to estimate lateral eddy diffusivities in the ocean and that these estimates are comparable to those obtained from RAFOS floats, where they overlap. Using the Southern Ocean State Estimate (SOSE) velocity fields to advect synthetic particles with imposed behavior that is "Argo-like" and "RAFOS-like" diffusivity estimates from both sets of synthetic particles agreed closely at the three dynamically very different test sites, the Kerguelen Island region, the Southeast Pacific Ocean, and the Scotia Sea, and support our approach. Observed cross-stream diffusivities at 1000 m, calculated from Argo float trajectories, ranged between 300 and 2500 $m^2\ s^{-1}$, with peaks corresponding to topographic features associated with the Scotia Sea, the Kerguelen Plateau, the Campbell Plateau, and the Southeast Pacific Ridge. These observational estimates agree with previous regional estimates from the Diapycnal and Isopycnal Mixing Experiment in the Southern Ocean (DIMES) near the Drake Passage, and other estimates from natural tracers (helium), inverse modeling studies, and current meter measurements. These estimates are also compared to the suppressed eddy diffusivity in the presence of mean flows. The comparison suggests that away from regions of strong topographic steering suppression explains both the structure and magnitude of eddy diffusivity but that eddy diffusivities in the regions of topographic steering are greater than what would be theoretically expected and the ACC experiences localized enhanced cross-stream mixing in these regions.

1. Introduction

The Antarctic Circumpolar Current (ACC) is a region of the world ocean where the eddy-driven contribution to meridional transport and thus the overturning circulation is thought to be of first-order importance, below the Ekman layers and above a sill roughly 2000 m deep. Observationally, quantifying these eddy fluxes is challenging as it requires long time series of both velocity and hydrographic properties and thus one has to resort to a transport parameterization, such as potential vorticity (PV) or thickness diffusion [*Marshall and Speer*, 2012; *Speer et al*., 2000]. This parameterization requires knowledge of the large-scale mean PV gradients and some estimate of an eddy diffusivity. Large-scale deployments of RAFOS floats or chemical tracers, as was done during the Diapycnal and Isopycnal Mixing Experiment in the Southern Ocean (DIMES), have been conducted to obtain observational estimates of the eddy diffusivity and to provide some ground truth to numerical models; however, these efforts are very expensive and only characterize eddy stirring in a limited region of the ocean. The goal of this study is to go beyond these regional studies and effectively characterize cross-stream mixing on a circumpolar-scale attention by using Argo data with its more extensive coverage.

Argo floats provide profiles of hydrographic properties between the surface and 2000 m and displacement vectors between subsequent surfacing locations approximately every 10 days. Previous studies have exploited the hydrographic data from Argo floats to estimate the eddy diffusivity [*Cole et al*., 2015; *Deng et al*., 2014] by calculating eddy mixing lengths from the observed property variances. However, these studies had to rely on either assumptions about the relationship between vertical and horizontal diffusivities or use eddy kinetic energy estimates from numerical model outputs to compute the diffusivity. Alternatively, the displacement vectors and the corresponding trajectories provide a rough estimate of the flow at the

© 2016. American Geophysical Union. All Rights Reserved.

parking depth (typically 1000 m) and can be used to obtain direct estimates of the lateral diffusivity at the parking depth [*Chiswell*, 2013; *Katsumata and Yoshinari*, 2010]. Both studies used Argo float displacements and assumed that the deviation from Lagrangian behavior generated by the Argo profiling cycle would limit the utility of the data over long time periods; hence, diffusivities were computed only over a short time period equivalent to a single Argo float cycle, 10 days. Recent studies [*LaCasce et al.*, 2014; *Klocker et al.*, 2012a] support the notion that the Lagrangian velocity autocorrelation function (the derivative of the eddy diffusivity) almost always displays a negative lobe on short time scale for oceanic flows. To obtain stable and reliable estimates of diffusivity, one must integrate the velocity autocorrelation beyond this negative lobe, which is generally on the order of 50–100 days. This is significantly longer than the Argo float cycling period used as the cutoff previously.

Here we reexamine the use of Argo float trajectories to estimate the lateral eddy diffusivity. We first check if systematic errors or bias are introduced to the diffusivity estimates due to the profiling nature of Argo floats since they strictly do not follow the same water parcel for a long period. This is tested by advecting synthetic trajectories, which behave either like Argo floats and profile every 10 days or like true Lagrangian floats (RAFOS float-like) that follow the same water parcel for long durations, using the Southern Ocean State Estimate (SOSE) velocity fields [*Mazloff et al.*, 2010]. These tests show that Argo float trajectories can be used to estimate lateral eddy diffusivity and produce diffusivity estimates that are comparable to RAFOS float trajectories. We then utilize Argo float trajectories to estimate the circumpolar distribution of lateral meridional and cross-stream eddy diffusivity. Finally, we compare the circumpolar distribution of cross-stream mixing to estimates provided by theories that incorporate suppression of mixing by the mean flow [*Ferrari and Nikurashin*, 2010; *Meredith et al.*, 2011].

2. Data Sets

2.1. Velocity Fields From Ocean Reanalyses for Particle Tracking

Numerical particle tracking requires high temporal and spatial resolution velocity fields. SatGEM with 1/3° resolution and Southern Ocean State Estimate (SOSE) with 1/6° resolution were both tested. We chose to use velocity fields from SOSE along with our particle advection routines as it provides better estimates of deeper velocities than SatGEM. However, the results of this study are not sensitive to this choice.

SOSE [*Mazloff et al.*, 2010] assimilates both in situ satellite and reanalysis data including Argo float, shipboard, and XBT temperature and salinity profiles; NCEP-NCAR reanalysis winds; satellite-derived sea surface temperatures and merged Topex/Poseidon-Jason-1 sea level anomalies. Note that while Argo hydrographic profiles are assimilated in SOSE, Argo float displacements (hence, velocities) are not. The resulting Southern Ocean State Estimate velocity fields offer 1/6° horizontal resolution, temporal resolution of 5 days, and a total of 42 depth levels unevenly distributed between the surface and 5575 m.

2.2. Argo and RAFOS Floats

Since the first deployments in the early 2000s, the Argo profiling float array has grown to cover all oceans with over 3000 active floats. Argo floats are normally configured to operate on an approximately 10 day cycle. Initially, the float sinks to a parking depth (typically 1000 m) over the course of 3–4 h. Then it drifts at this parking depth for 8–9 days before descending to around 2000 m. The float then ascends to the surface while measuring a profile of the water column properties over the course of about 6 h. Finally, it drifts on the surface while transmitting data to satellites and then recommences its cycle. This transmission takes less than an hour for newer generation floats using the Iridium communications system and 9–12 h for floats using the older ARGOS system.

We used the November 2014 delayed time version of the YoMaHa'07 data set [*Lebedev et al.*, 2007] and identified approximately 1500 Argo floats with trajectories passing between 45°S and 65°S. 1300 of these spent greater than 150 consecutive days south of 45°S, delivering a total of 15,500 displacement vectors (Figure 1, top). Twenty percent of these floats, producing 35% of all trajectory data, were equipped with the Iridium communications systems. Eighty-nine percent of Argo cycles ranged between 9 and 11 days in length, with a mean of 9.9 days. Time spent at the surface varied between less than 1 and 24 h, with a mean time spent on the surface by ARGOS-equipped floats of 9.9 h. Ninety-one percent of these trajectories had a programmed parking depth between 900 and 1100 m. While YoMaHa'07 does not record the parking

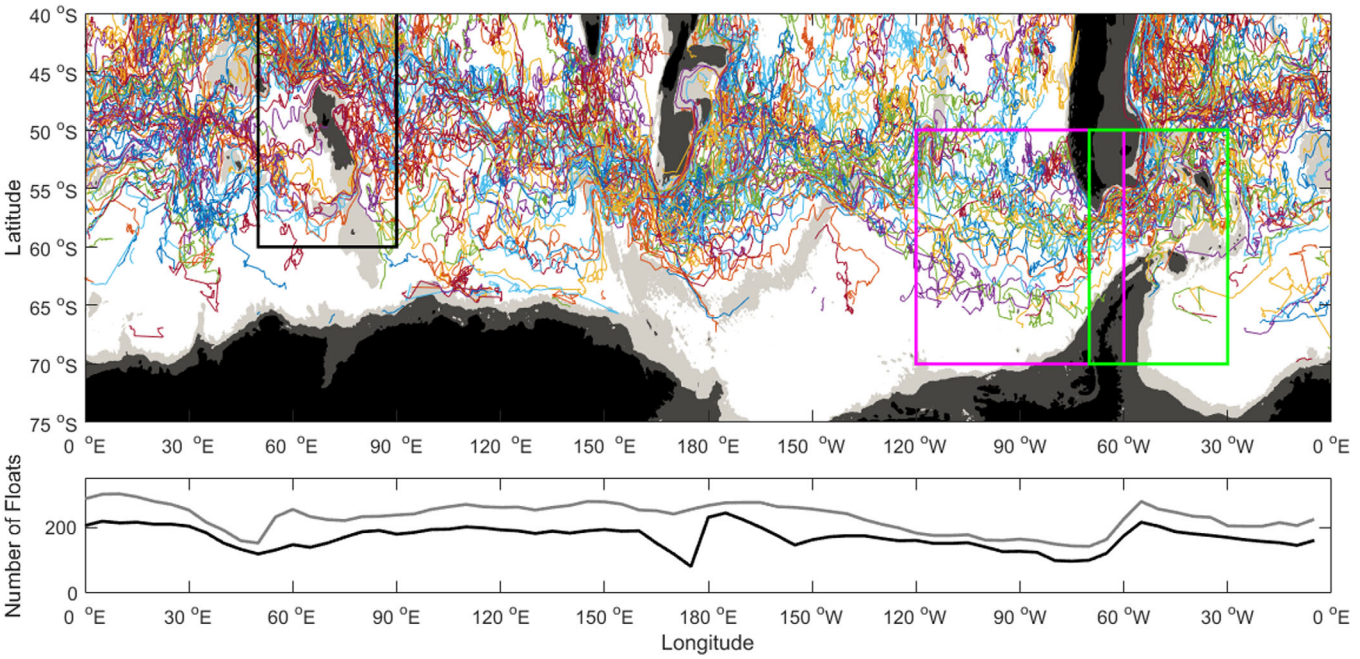


Figure 1. Map showing 500 of the 1597 Argo float trajectories (top) used in this study. Areas shaded light gray indicate depths of between 1000 and 3000 m; dark gray indicates depths of less than 1000 m, and black indicates land. Rectangles indicate the domains of the numerical experiments described in sections 3.2 and 4.1 (black marks the Kerguelen Plateau; green the Scotia Sea and pink DIMES region). Number of floats (bottom) present in each longitude bin (gray) and the number of floats in each bin which spent more than 150 days south of 45°S (black).

depth actually achieved on each cycle, examination of the ANDRO data set [*Ollitrault and Rannou*, 2012] indicates that 80% of Argo cycles achieved a parking depth within that range.

In addition, we employ a set of 83 acoustically tracked RAFOS floats from the DIMES experiment, which were deployed along a line at 110°W between 55°S and 65°S and drifted at an approximate depth of 1500 m [*LaCasce et al*., 2014]. These will be used to estimate diffusivities in the South Eastern Pacific, to provide an observational test case to validate the diffusivities obtained from Argo floats.

2.3. Sea Surface Height Data

Maps of mean dynamic topography [*Lagerloef et al*., 1999; *Rio and Hernandez*, 2004] produced by the SSALTO/DUACS (Segment Sol multi-missions dALTimetrie, d'orbitographie et de localisation précis/Data Unification and Altimeter Combination System) program were sourced from AVISO. These time-varying fields of absolute dynamic topography are derived by merging sea surface height (SSH) data from multiple satellite missions (including Jason 1 and 2, Topex/Poseidon, and Envisat). The resulting velocity fields have a 1/3° spatial resolution and 1 day temporal resolution.

3. Methods

3.1. Estimating Eddy Diffusivities

In this study we computed eddy diffusivities by following three different methods as described below.

3.1.1. Computing Meridional Diffusivity From Float Trajectories

The use of Lagrangian data to calculate eddy diffusivities was extended to nonhomogeneous oceanic flow by *Davis* [1991a, 1991b]. Absolute eddy diffusivity (alternatively known as single-particle diffusivity) is a tensor defined as

$$K_{ij} = \langle \boldsymbol{u}'_i(t)\boldsymbol{d}'_j(t)\rangle,$$

where $\boldsymbol{u}'$ and $\boldsymbol{d}'$ are vectors of eddy velocity and particle displacement (with corresponding total velocity **u** and distance to release point **d**), i and j indicate a set of orthogonal axes, t denotes time, and $\langle\ \rangle$ denotes an ensemble average over all particles or floats. This ensemble average is generally performed by averaging

over all floats/particles that pass through a geographical region and the estimated diffusivity is the averaged diffusivity for the region. Similar averaging has been applied for the other diffusivity estimation techniques used in this study. *Swenson and Niiler* [1996], *Zhurbas and Oh* [2004, 2003], *Sallee et al*. [2011], *Chiswell* [2013], *Griesel et al*. [2013], *LaCasce et al*. [2014], to name a few, have performed similar averaging in previous observational and numerical studies.

If we consider the case of zonal flow with the i and j axes aligned with the Cartesian x and y axes, respectively, then $K_{jj} = K_m$, the meridional diffusivity. K_m can be expressed as a number of equivalent expressions [*LaCasce*, 2008], including the correlation between particle velocity and displacement

$$K = \langle u(t)[y(t) - y_0] \rangle.$$

The integral of the autocorrelation of velocity (where τ denotes time lag)

$$K = \int_0^t u([y(t) - y_0], t) u([y(t) - y_0], \tau) d\tau.$$

Otherwise, the derivative of single-particle dispersion $\langle [y(t) - y_0]^2 \rangle$

$$K = \frac{1}{2} \frac{d}{dt} \langle [y(t) - y_0]^2 \rangle, \tag{1}$$

where y(t) denotes the particles' meridional position as a function of time and y_0 denotes the particles' position at release. Sometimes y_0 is replaced by the position of the center of mass of the particle ensemble to calculate the diffusivity relative to the mean motion of particle ensemble.

However, in practice most of these definitions result in noisy estimates of diffusivity [*LaCasce et al*., 2014]. We instead follow a method applied in *LaCasce et al*. [2014, equation (9)] which assumes that the growth of the dispersion, the variance of displacements, is linear at long times and can be simply fitted by the form

$$K_m = \frac{\langle (y(t) - y_0)^2 \rangle}{2t}. \tag{2}$$

To estimate the uncertainty in our diffusivity estimates, we used a bootstrap approach similar to *Klocker et al*. [2012b] and *Griesel et al*. [2010]. Within our area of interest we dropped a randomly selected float or particle trajectory then resampled the remaining data, allowing for duplicates, before recomputing the diffusivity. This procedure was repeated 100 times and the uncertainty in the diffusivity was then taken as the resulting two standard deviation range.

3.1.2. Computing Cross-Stream Diffusivities Using SSH-Contours

To compute cross-stream diffusivities from single-particle statistics, we follow an approach similar to *Sallee et al*. [2011]. Assuming approximate equivalent barotropic flow, we identify the sea surface height (SSH) contour on which a given particle was released. At each subsequent time step, we then find the minimum distance up (positive) or down (negative) the SSH gradient between the release SSH and the particle (Figure 2). We use this to construct time series of particle displacements relative to initial SSH-contours—cross-stream displacement, $d_{cc}(t)$. Assuming that the cross-contour spreading is Gaussian and following the same arguments as described for the meridional case above, the cross-stream eddy diffusivity can be computed as

$$K_{cc} = \frac{\langle d_{cc}(t)^2 \rangle}{2t}. \tag{3}$$

We use SSH-contours defined by a 20 day moving average of the SSH fields for calculating the cross-stream displacement time series. The effect of this choice compared to different averaging periods is discussed further below. Error analysis was conducted in the same fashion as used when estimating the meridional diffusivity (see above).

3.1.3. Computing Cross-Stream Diffusivities From Relative Dispersion

It can be shown analytically that the principal components of the diffusion tensor, for a system with linear shear, behave such that the minimum of the principal components asymptotes to the background isotropic diffusivity and the maximum of the principal components asymptotes to the shear enhanced diffusivity in the direction of the mean shear of the system [*Bolster et al*., 2011; *LaCasce*, 2008]. *Zhurbas and Oh* [2003] applied this idea and calculated along and across mean flow diffusivities using the average of the rate of

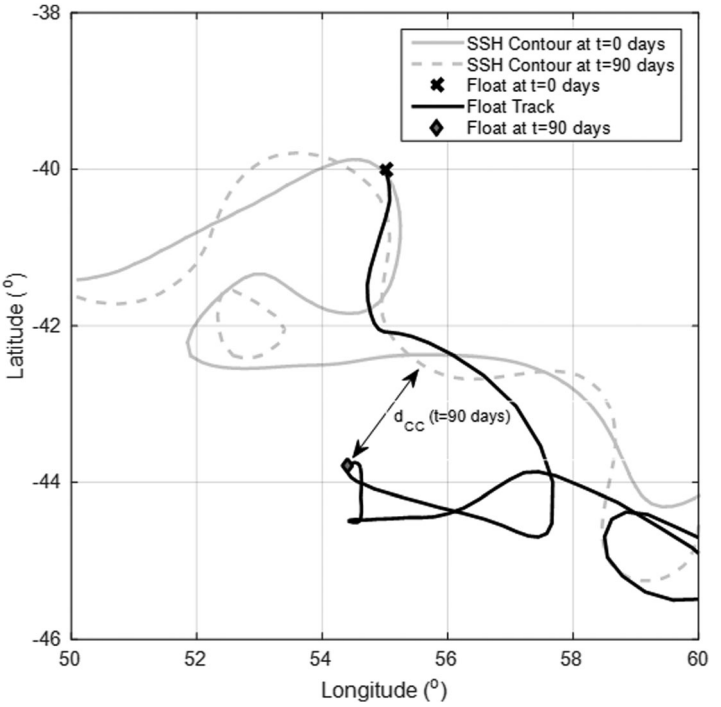


Figure 2. Example of one float track (black) with sea surface height contours corresponding to float release (t = 0 days, gray solid line) and at t = 90 days (gray dashed line) with the cross-contour distance at 90 days (d_{CC}) indicated.

change of the principal components of the single-particle dispersion tensor and the principal component of the diffusivity tensor.

It is also straightforward to show that the relative diffusivity or two-particle diffusivity asymptotes to twice the single-particle diffusivity when the particle pair velocities become decorrelated with each other [*Klocker et al.*, 2012b; *LaCasce*, 2008]. This decorrelation happens at large length scales (greater than maximum eddy length scales) and is a necessary criterion that needs to be satisfied for particle motions to behave as random walks and thus for the eddy transport to be approximated as a diffusive process. Relative dispersion calculations provide more degrees of freedom than the single-particle estimates to the diffusivity calculation such that N floats provide N(N-1)/2 pairs for calculating relative diffusivity. As we are interested in the long-term eddy diffusivities after the pair motions have become decorrelated, we do not need to use closely spaced particles when considering initial pairs [*LaCasce and Ohlmann*, 2003]. All pairs that are either initially decorrelated or decorrelate in finite time, and are not sampling over extremely different length scales, can be considered in the ensemble used for averaging. We also expand the idea of decorrelated motions further by assuming that decorrelated motions in space or time are equivalent. Hence, we can construct pairs with floats that pass through a region at different times. This notion works as long as there are no large seasonal (low-frequency) motions associated with the mean flows, which can possibly bias the diffusivity calculations.

We estimate the cross-mean flow diffusivity by following the principal component approach applied to the relative diffusivity tensor, in contrast to the across SSH diffusivity calculation described previously. These two methods should give similar results, provided that the shear in the system is approximately linear and the SSH contours provide a good approximation to the mean flow at 1000 m.

At each time step we construct a relative dispersion matrix

$$\begin{bmatrix} \langle d_x{}^2 \rangle & \langle |d_x| \cdot |d_y| \rangle \\ \langle |d_x| \cdot |d_y| \rangle & \langle d_y{}^2 \rangle \end{bmatrix},$$

where d_x and d_y denote the zonal and meridional components of particle separation for each pair, and $\langle\ \rangle$ indicates averaging over all pairs.

We then find the two eigenvalues (denoted λ below) of the dispersion matrix at each time step and use them to compute relative diffusivities

$$K_{rel}(t) = \frac{\lambda(t) - \lambda_0}{2t}.$$

As noted above, the asymptotic relative diffusivity as the pair velocities decorrelate is twice the absolute diffusivity [*LaCasce*, 2008]; hence,

$$K(t) = \frac{K_{rel}(t)}{2} = \frac{\lambda(t) - \lambda_0}{4t}. \quad (4)$$

The smaller of the two resulting absolute diffusivities is taken to represent cross-stream diffusivity.

When applying this method to the Argo and RAFOS data, float-pairs were selected only when the two floats were less than 100 km apart at the time they entered, or were deployed within, each longitude bin. We tested the effects of using a lower maximum limit on initial particle separation (not shown) and found that the long-term mean diffusivities displayed little sensitivity to this choice. However, the uncertainty increased by up to a factor of 3 for initial particle separations less than 20 km, as the number of pairs contributing to the calculation is dramatically reduced.

We assessed the uncertainty in this diffusivity estimate using a bootstrap process. A float was randomly selected, all pairs including that float were dropped, the remaining data were resampled allowing for repetition, and another estimate of diffusivity produced. This process was repeated 100 times with randomly selected floats, and then the uncertainty in the diffusivity was taken as the resulting two standard deviation range.

3.2. Numerical Particle Tracking

We conduct numerical particle tracking experiments in three regions (shown in Figure 1) of the Southern Ocean to validate the methods discussed above and test the hypothesis that Argo floats can be used to compute long-term eddy diffusivities. First, we concentrate on the DIMES region (60°W–120°W and 50°S–70°S), in the South East Pacific through to the Drake Passage; this region displays relatively simple zonal flow. Next, we consider the Drake Passage and Scotia Sea (30°W–70°W), a region of stronger complex flow dominated by topographic interactions, eddies, and meanders. Finally, we consider the Kerguelen Plateau region (50°E–90°E and 30°S–60°S) that is dominated by the northward deflection of the Subantarctic front around the plateau and enhanced eddy activity both to the north and downstream of the plateau. In each region we conducted three varieties of numerical particle experiments: Argo-like particles drifting at 1000 m and cycling between the surface and 2000 m, isobaric particles at a depth of 1500 m, and isobaric particles spread between 700 and 1500 m. These experiments allow us to compare estimates of mixing from the Argo-like particles to "true" lateral diffusivities obtained by the 1500 m isobaric particles. The 700–1500 m release of isobaric particles provides an indication of how sensitive diffusivity estimates are to floats that might not equilibrate at the same depth level (similar to the DIMES experiment). Note that trial runs were also conducted with isobaric particles at 1000 m depth. The resulting diffusivities were not distinguishable from the 1500 m isobaric experiments.

The goal of our numerical experiments is to test our methods and the appropriateness of hypothesis that Argo floats can be used to estimate diffusivities. We do not want to produce extensive estimates of diffusivity from the numerical model at the finest resolution possible; instead, we designed the experiments to produce trajectories that will be similar to those obtained from observations. In each of the Argo-like and 1500 m isobaric particle experiments, a total of 3300 floats were released along a line of constant longitude over an interval of 10° of latitude in three bursts at 3 month intervals (1 June, 1 September, and 1 December 2005). The second isobaric particle experiment used the same temporal and latitude/longitude release configuration, but released a total of 33,000 particles evenly spread across 10 depth levels between 700 and 1500 m. Particle trajectories were integrated forward until either 1000 days or until all particles exited the region covered by the SOSE velocity fields.

For the Argo-like experiment we assume an "idealized" 10 day cycle. All particles were released at the surface and then descended to a parking depth of 1000 m over the course of 3 h, floats remained at parking depth for 9 days before descending to 2000 m and profiling to the surface over the course of 9 h, the cycle completes with the float spending 12 h on the surface. The output of particle trajectories from each experiment was then used to estimate diffusivities as described in the previous section.

Particle tracking was conducted using the Connectivity Modelling System (CMS) v1.1 revision 169 [*Paris et al*., 2013]. This software uses a fourth-order Runge-Kutta integration method to advect particles through a 3D, time-evolving velocity field. Velocities fields evolved between the 5 day interval SOSE fields using linear interpolation.

While CMS can be configured to move particles up or down the water column using prescribed buoyancy or vertical velocity, neither was suitable for modeling Argo floats. Use of vertical velocities was ruled out because the temporal resolution of SOSE fields was too coarse (5 day resolution) to represent the vertical motions of an Argo float. Use of the buoyancy module was not possible, as the present stable version of CMS v1.1 does not allow the buoyancy of particles to evolve in time. We instead employed the ontogenetic vertical migration module, in which evolution of a particle's depth is controlled by a matrix specifying the probability of a particle being at a particular depth during a given time interval. We configured the vertical migration matrix to reproduce the "generic" Argo cycle described above. During the descent and profiling phases we divided time into half hour blocks, during each half hour block each particle was randomly assigned a depth (and hence velocity) within a 100 m window around the expected depth assuming a 10 cm s^{-1} descent or ascent rate. At parking depth and at the surface particles were assumed to maintain a constant depth, with no spread around it.

The CMS was run with a time step of half an hour and particle locations were saved at 2 day intervals. In order to get divergence between particles initialized at the same start point, it is necessary to include small background diffusivity; for this study we assumed a background diffusivity of 1 m^2 s^{-1}. The resulting perturbations to particles were then applied by the CMS at each time step. It should be noted that SOSE produces ocean diffusivities that are 10–20% lower than estimated ocean values. Thus, we have only used SOSE to test our hypothesis under a range of different flow conditions.

4. Results

In this section, we test the hypothesis that trajectories following Argo float cycles can be used to estimate long-term diffusivity that is comparable to that obtained from RAFOS floats. In addition, we estimate the diffusivity in the Southeast Pacific Ocean using Argo floats that passed through the region and compare it to the estimates obtained from RAFOS float observations that were collected as part of the DIMES experiment. We then extend the diffusivity calculations using Argo floats to the entire Southern Ocean, focusing on its circumpolar variations, and compare it to some theoretical results that have been presented in previous studies.

4.1. Numerical Test Cases

Numerical experiments at three test sites (Figure 1) were selected because they represent three dynamically distinct flow regimes: the South East Pacific sector of the Southern Ocean dominated by relatively smooth and zonal ACC flow; the Scotia Sea dominated by strong eddy activity and the constriction of the ACC by Drake Passage, and the region near the Kerguelen Plateau dominated by a splitting of the ACC into northern and southern branches.

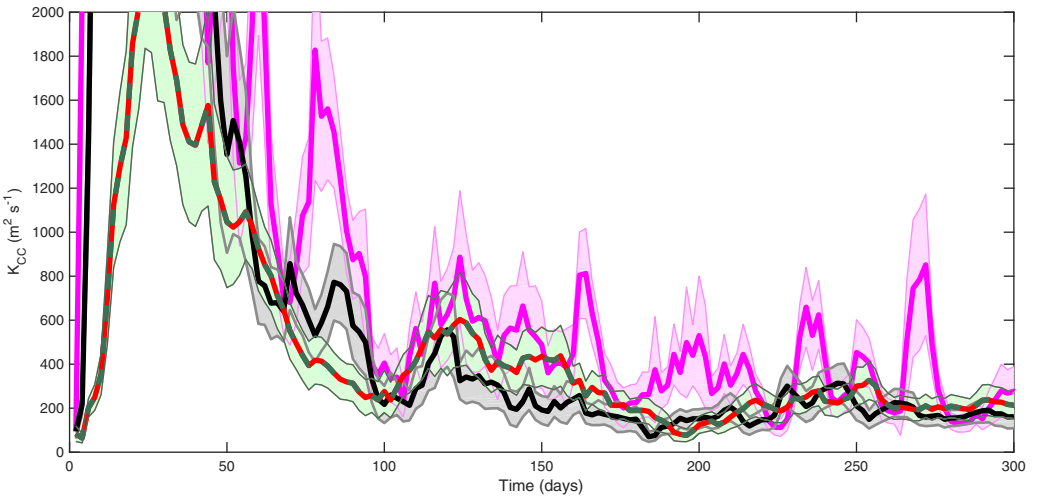


Figure 3. Cross-contour diffusivity in the South East Pacific as a function of time for the raw 1 day resolution SOSE SSH fields (pink) and 20 day (black), 40 day (red), and 60 day (green) averaged SSH fields.

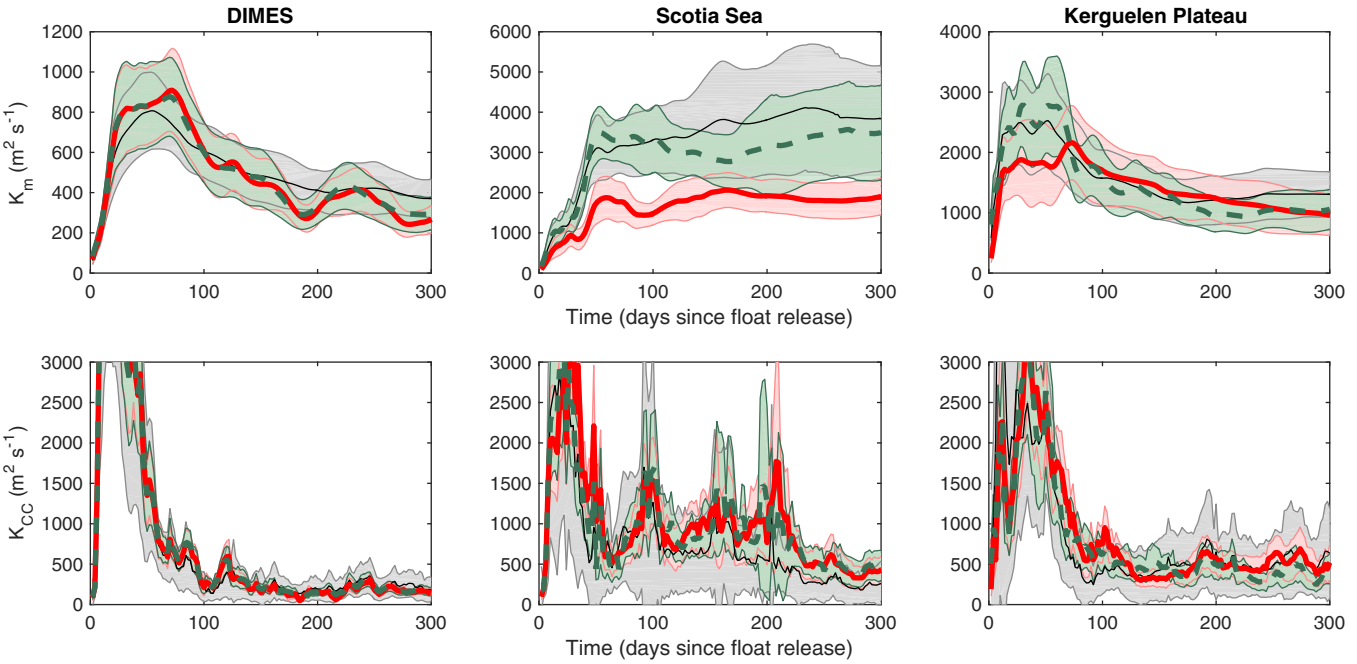


Figure 4. Diffusivities versus time for meridional (top) and cross-contour (bottom) eddy diffusivities from numerical particle tracking in SOSE velocity fields near the Kerguelen Plateau; in the Scotia Sea and in the DIMES region. Black indicates the multiple depth isobaric Lagrangian release, red the 1500 m isobaric Lagrangian release and green the Argo release. Shaded areas indicate 2σ confidence intervals estimated using the bootstrap procedure described above.

Diffusivities for the numerical test cases were computed in the same manner as the observational data (below). For single-particle diffusivities all particle tracks in the region of interest were used instead of only particles released from the same location, while for two-particle diffusivities all pairs of appropriate initial separation were used regardless of if the particles forming each pair were released at the same time.

Before proceeding, we need to determine the appropriate level of smoothing to apply to the SSH fields for the K_{cc} calculations. Smoothing over too short a period is liable to increase the uncertainty while excessively long smoothing is liable to misrepresent changes in the larger-scale flow regime as diffusivity. Tests using numerical particle tracks in the SOSE velocity fields (Figure 3) indicated that SSH fields smoothed for less than about 20 days display excessive noise, while asymptotic diffusivities for smoothing periods of 40–60 days were not statistically distinct from the 20 day diffusivities. Hence, in the following cross-contour diffusivity will be estimated relative to 20 day SSH contours.

Diffusivity as a function of time for the three numerical test regions and three varieties of numerical particles (isobaric particles at 1500 m, Argo-like particles with a parking depth of 1000 m and profiling to 2000 m, and isobaric particles spread vertically between 700 and 1500 m) are shown (Figure 4). Similar trials were performed with isobaric particles at 1000 m but are not shown, as they did not differ within error from the 1500 m test case. As shown in previous studies there is an initial strong transient response in diffusivity that settles to an asymptotic value around 100 days postrelease, as the integration time becomes long compared to the negative lobe in the autocorrelation function.

Meridional diffusivities (K_m) from Argo-like and both isobaric particle trajectories from the three test sites (Figure 4, top row) agreed within 2σ confidence intervals. Confidence intervals on meridional diffusivity were of similar magnitude for all experiments. The "asymptotic" (time $>$ 100 days) meridional diffusivities were found to be larger than the corresponding cross-contour diffusivities, which is discussed below.

Cross-contour diffusivities (K_{cc}) were also found to agree within confidence intervals at all three test sites (Figure 4, bottom row). The cross-contour diffusivities showed narrower confidence intervals on the Argo-like and isobaric particles at 1500 m experiments when compared to the mixed depth (700–1500 m) isobaric particles. The Scotia Sea results displayed a number of smaller peaks after the initial transient response had decayed, possibly caused by a small number of particles found close to the coast. These particles had

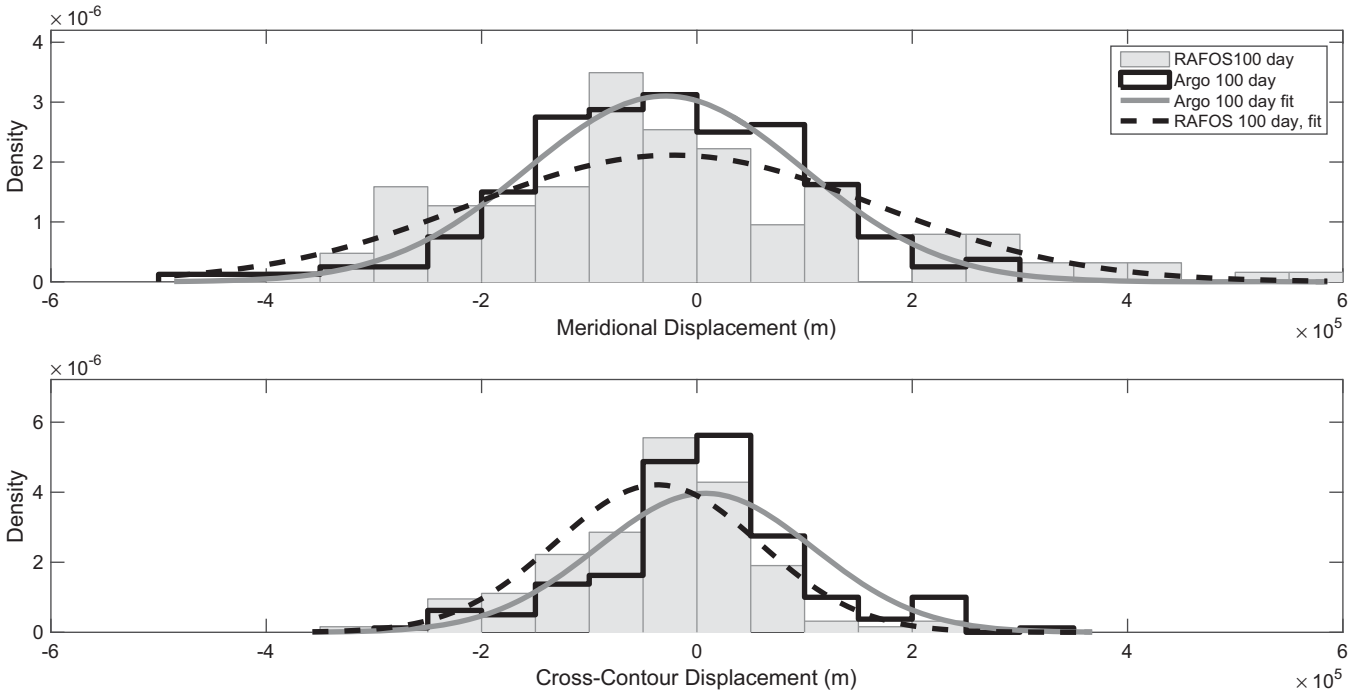


Figure 5. Probability density functions of meridional (top) and cross-stream (bottom) float displacements 100 days after float release for Argo and RAFOS floats deployed between 105°W and 100°W. Bars indicate the observed PDFs and lines Gaussian fits to the data.

been released on SSH contours which did not pass through the Drake Passage at all time steps, resulting in a small number of abnormally high cross-contour displacements.

These results confirm that under different flow conditions observed in the Southern Ocean, Argo floats are a suitable source of trajectory data for estimating long-term eddy diffusivities.

4.2. Comparison With RAFOS Observations in the DIMES Region

We compare the diffusivities from trajectory observations in the south-east Pacific Ocean, from both Argo float data and DIMES RAFOS float data. The calculation of diffusivity depends on the assumption that the displacement of floats is Gaussian. We test this assumption by applying Gaussian fits to the observed probability density functions (PDFs) of float displacement at 100 days postrelease (Figure 5). Visual comparison suggested good agreement between the fitted and observed PDF of both meridional and cross-stream displacements, which was confirmed by the application of Kolmogorov-Smirnov test [*Massey*, 1951; *Rohatgi and Ehsanes Saleh*, 1976] to PDFs. The PDFs also clearly demonstrate that the cross-contour method produces lower variance and diffusivities than the meridional approach, as the cross-contour approach is not affected by the slow meridional mean flow.

Meridional diffusivity (K_m) and both single (K_{cc}) and two-particle ($K_{rel}/2$) cross-stream diffusivities as a function of time were estimated from Argo and RAFOS float trajectories (Figure 6). Both meridional and cross-stream diffusivities display an initial transient peak before settling down to a constant value after approximately 100 days. Both meridional and single-particle cross-stream diffusivities estimates obtained by Argo and RAFOS floats agree within two standard deviation confidence intervals over the entirety of the record. The two-particle cross-stream diffusivities ($K_{rel}/2$) agree with the single-particle cross-contour diffusivity (K_{cc}) from the corresponding data set, but disagree between the two data sets. The two-particle cross-stream Argo diffusivity being approximately 100 $m^2\ s^{-1}$ smaller than the RAFOS diffusivity at times after the initial transient response has subsided. This discrepancy could be a result of the vertical shear associated with the ACC enhancing the diffusivity for the RAFOS floats [*Balwada et al.*, 2016], which were distributed in the vertical at variable equilibration depths (500–2000 m).

Similar to the results presented in Figure 4, the cross-contour diffusivities are smaller than the meridional diffusivities. We see that asymptotic values of K_{cc} are about 400–500 $m^2\ s^{-1}$, while K_m is typically between

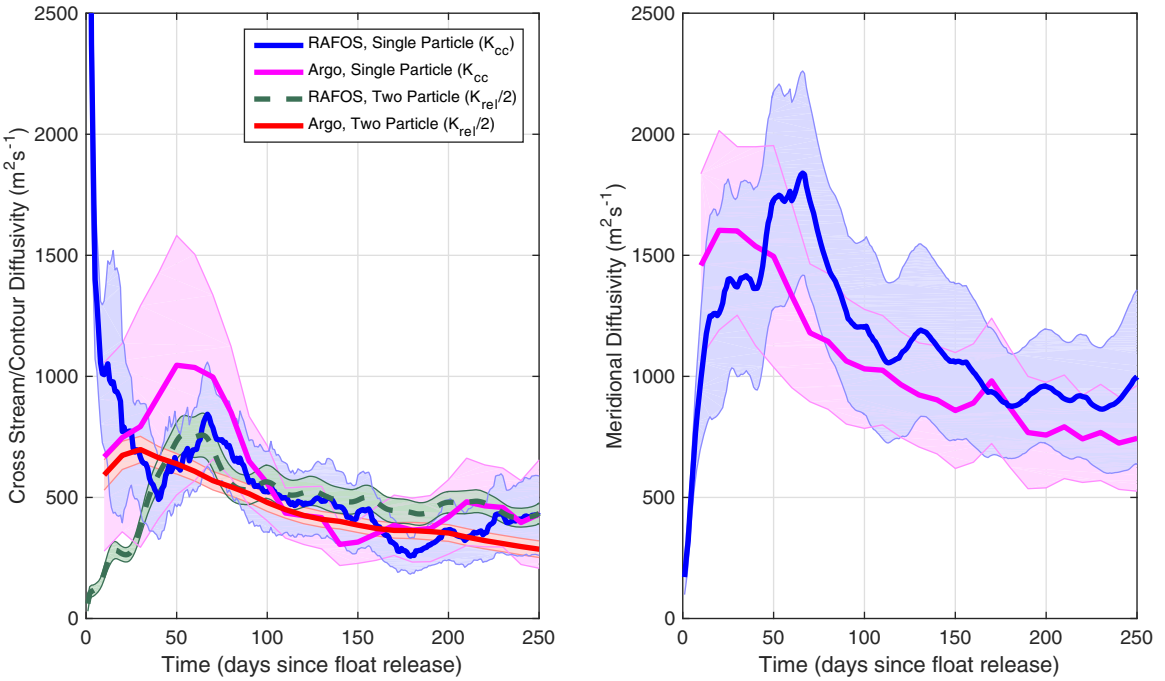


Figure 6. Mean cross-stream (left) and meridional diffusivities (right) estimated as a function of time since float release for Argo and RAFOS floats released between 105°W and 100°W. Shaded regions indicate two standard deviation confidence intervals estimated from bootstrap resampling.

700 and 1200 $m^2\ s^{-1}$ (Figure 6). This range of values is consistent within errors with estimates upstream of the Drake Passage made using tracers [*Tulloch et al.*, 2014]. This implies that even in a region of relatively zonal flow, like the South East Pacific sector, using meridional diffusivities as an approximation of cross-stream mixing results in an overestimate of 50–100%. These errors are likely to be larger in regions of either intense eddy activity or substantial meridional flow.

We again conclude that it is possible to obtain estimates of lateral eddy diffusivity from Argo floats that agree closely with estimates from RAFOS floats. This is consistent with a theoretical examination (Appendix A) of the effect of using profiling floats on diffusivity estimates, in which we conclude that in the Southern Ocean regime the errors introduced by using an ARGOS-equipped profiling float are comparable to the errors inherent in estimating diffusivity from RAFOS float or surface drifter trajectories.

4.3. A Circumpolar Application

We split the Southern Ocean into 5° longitude by 20° latitude (45°S–65°S) bins and then identified all Argo floats that enter each bin (Figure 1, bottom). Segments of the Argo float trajectories starting in each bin, and extending up to 15° downstream, were isolated and time series of meridional, zonal, and cross-contour displacement produced. Meridional, single-particle cross-contour and two-particle cross-stream diffusivities were then computed using equations (2)–(4).

We examined the PDFs of float displacement 150 days post-release in the bins, examples from the Kerguelen Plateau region and the Scotia Sea are shown in Figure 7. Consistent with our findings in the DIMES region and SOSE velocity fields the cross-contour displacement consistently produced Gaussian PDFs. PDFs of meridional displacement, on the other hand, were more variable with Gaussian distributions in some regions (e.g., 60°E, near the Kerguelen Plateau) and distinctly non-Gaussian distributions in other regions (e.g., the Scotia Sea). This further suggests that properly resolving the cross-stream component of displacement is essential.

4.3.1. The Circumpolar Distribution of Horizontal Mixing

Diffusivity as a function of longitude (Figure 8) shows strong regional variations, consistent across the different diffusivity estimates used here. The single-particle cross-contour and two-particle cross-stream diffusivities were found to vary between 300 and 2500 $m^2\ s^{-1}$. They agree within 2σ confidence intervals everywhere, with the exception of two regions centered on 130°E and 70°W. The meridional diffusivity

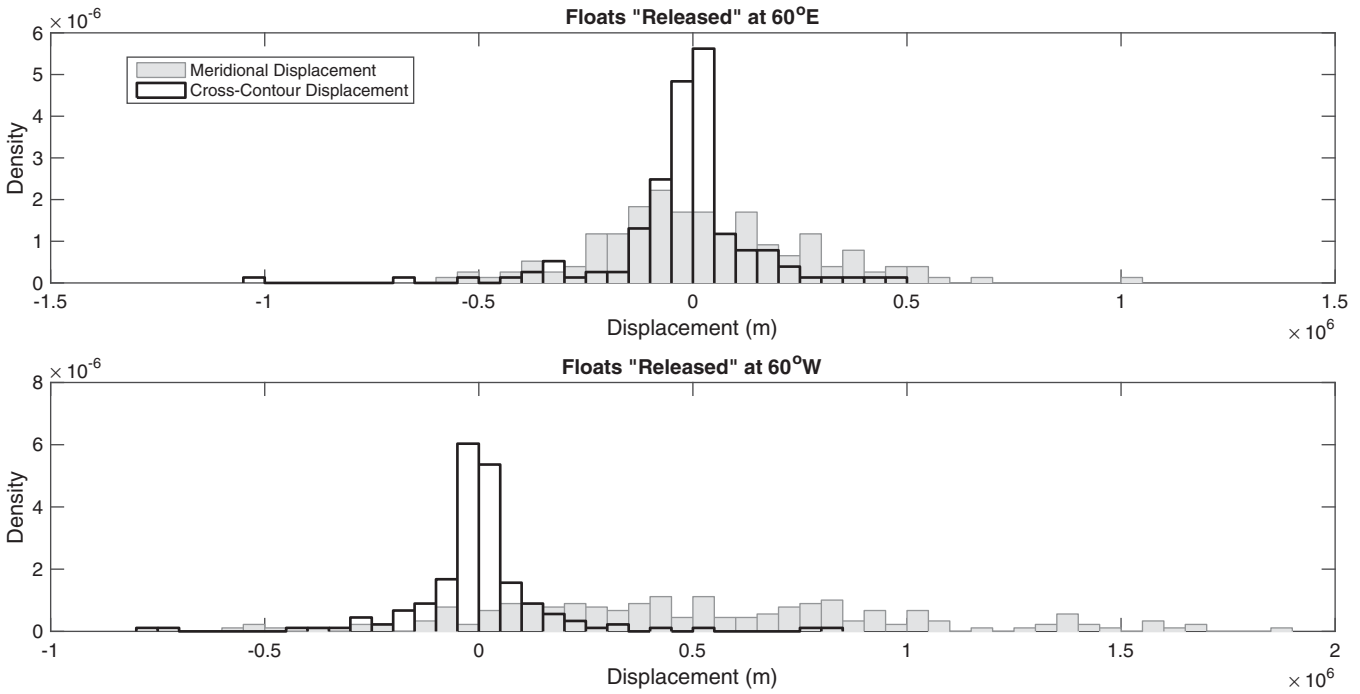


Figure 7. Probability density functions of meridional and cross-contour float displacements for the Kerguelen Plateau region (top) and the Scotia Sea (bottom) 150 days postrelease.

varied between 1000 and 10,000 $m^2\ s^{-1}$, affected strongly by the mean shear. All diffusivities estimated from Argo floats displayed a similar pattern of regional variability, with local maxima near 30°E, 70°E–80°E, 160°E, 130°W, and 60°W. These peaks correspond approximately to the Aghulas retroflection, the Kerguelen Plateau, the Campbell Plateau, part of the Pacific-Antarctic ridge, and the Scotia Sea, known to be sites of significant eddy activity.

We compare our diffusivity estimates to those available from previous studies (Figure 8). These include estimates from a mooring array [*Phillips and Rintoul*, 2000] south of Australia; estimates from the use of natural He isotopes as passive tracers [*Naveira-Garabato et al.*, 2007] in the Scotia Sea; estimates from an inverse model based on tracer distributions [*Faure and Speer*, 2012] in the Pacific sector; and estimates from RAFOS float observations [*LaCasce et al.*, 2014] in the DIMES region. Our cross-stream diffusivities agree closely with previous studies in the DIMES region and Scotia Sea. Mean values for both K_{cc} and $K_{rel}/2$ are high relative to estimates from *Faure and Speer* [2012] and *Phillips and Rintoul* [2000]. The single-particle estimate overlap with their estimated ranges at the very limits of the 2σ confidence intervals, while the two-particle estimate did not agree with these prior studies within confidence intervals. This is likely an effect of the different geographic scopes of the studies. *Phillips and Rintoul* [2000] estimate the diffusivity from a closely spaced array of four moorings located near 50°30′S, 143°E, in proximity to a front. *Faure and Speer* [2012] estimated the diffusivity from an inverse model that was principally focused on the south-east Pacific north of the ACC. Their estimate likely represents lower diffusivities from the interior of the south-east Pacific. We conclude that our estimates of cross-stream diffusivity are broadly consistent with previous studies in the Southern Ocean.

4.3.2. Comparison to Theory

Previous studies [*Ferrari and Nikurashin*, 2010; *Meredith et al.*, 2011] have considered the effect of a broad zonal mean flow along with propagating eddies in a quasi-geostrophic framework on eddy diffusivities. They showed that the mean flow suppresses the diffusivity that would otherwise be expected for the eddy field in isolation. These studies assumed a scale separation between the scale of mean flow and eddies—the width of the jet is much larger than the radius of the eddies. However, other studies [*Rypina et al.*, 2007] have shown suppression to be at work even in the absence of scale separation. *Ferrari and Nikurashin* [2010] used a linear stochastic model to derive a testable expression for eddy diffusivity, with the assumption that eddy forcing is monochromatic in wave number. The net result is that the mean flow (U_M) acts to produce an effective diffusivity (K_{eff}) smaller than the diffusivity (K_0) expected in the absence of mean flow

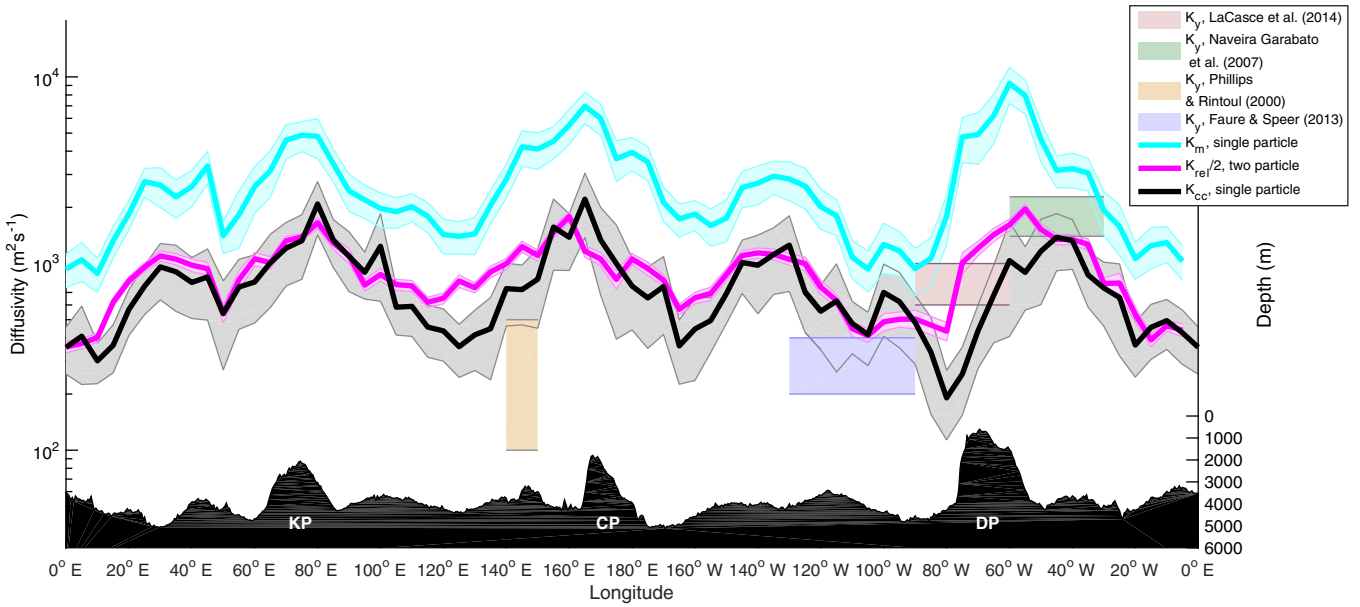


Figure 8. Circumpolar estimates of mean eddy diffusivity between 100 and 200 days postrelease from single and two-particle statistics (cyan K_m; black single-particle diffusivity, K_{cc} and pink two-particle diffusivity $K_{rel}/2$) compared to diffusivity ranges observed in previous studies (green, blue, purple, and brown shaded regions). Mean depth between 45°S and 60°S is shown as the black, shaded region. Shaded areas around our estimates of diffusivity indicate 2σ confidence intervals. The label KP, CP, and DP indicate the Kerguelen Plateau, Campbell Plateau, and Drake Passage, respectively.

$$K_{\text{eff}} = \frac{K_0}{1+\gamma^{-2}k^2(U_M-c)^2},$$

where K_0 is defined as follows and is the diffusivity expected based on standard mixing length arguments.

$$K_0 = \frac{k^2}{(k^2+l^2)}\frac{EKE}{\gamma}.$$

EKE denotes the eddy kinetic energy, γ the linear eddy damping rate—representing nonlinear damping through eddy-eddy interactions, c denote the eddy phase speed, and (k,l) are the zonal and meridional horizontal wave vector of the eddy field. K and l are defined as $2\pi/L_x$ and $2\pi/L_y$, where L_x and L_y are the length scales of the dominant eddies.

If we follow the assumption from *Ferrari and Nikurashin* [2010] that the ACC flow can be decomposed into near-circular (isotropic) eddies superimposed on a broad mean flow, k and l are approximately equal, then K_{eff} becomes

$$K_{\text{eff}} = \frac{\text{EKE}}{2\gamma(1+\gamma^{-2}\text{k}^2(U_M-c)^2)}.$$

With the exception of the eddy damping rate, the other parameters required to estimate the effective diffusivity can be obtained directly from existing data sets. We follow previous studies based upon sea surface altimetry observations [*Ferrari and Nikurashin*, 2010; *Meredith et al.*, 2011] which obtain an estimate for the eddy damping rate as

$$\gamma^{-2}\text{k}^2 \approx \frac{4}{\text{EKE}}.$$

In which case the expressions for effective diffusivity becomes

$$K_{\text{eff}} = \frac{\sqrt{EKE}}{k\left(1+4\frac{(U_M-c)^2}{EKE}\right)}. \quad (5)$$

We will refer to the factor $\frac{1}{1+4((U_M-c)^2/EKE)}$ as the suppression factor, which determines the fraction by which the standard mixing length theory diffusivity (K_0) is reduced in the presence of mean flow.

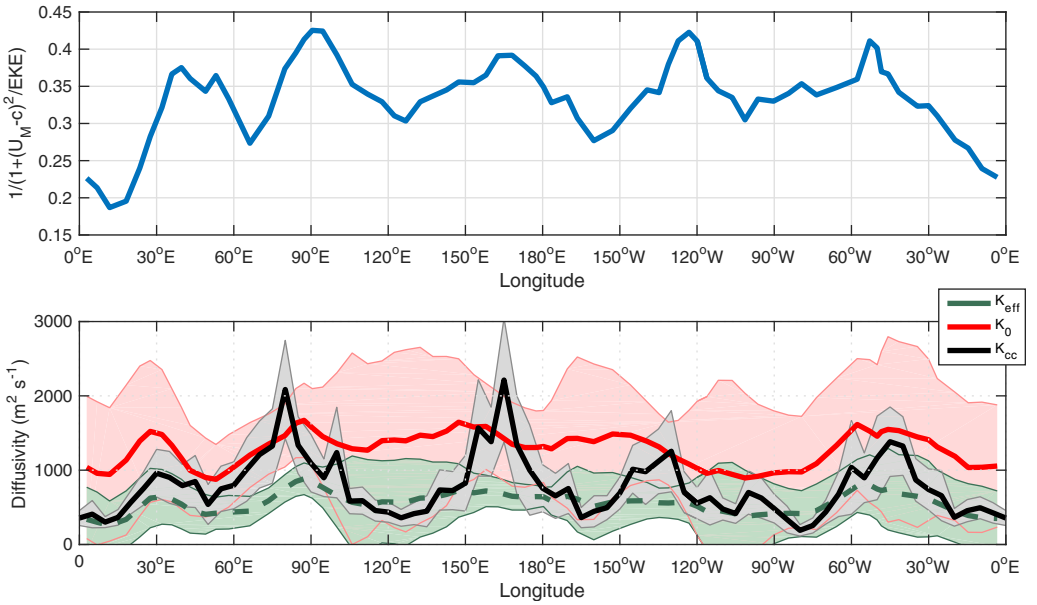


Figure 9. Suppression factor as a function of longitude (top). Observed single-particle diffusivities (black, shaded area 2σ range) and theoretical diffusivities (green K_{eff} and red K_0. Shaded areas indicate 2σ range) from equation (5) as a function of longitude (bottom).

We produced a gridded field of U_M by averaging YoMaHa'07 velocities in regular $1^\circ \times 1^\circ$ bins and obtained gridded fields of eddy length scales and phase speed from SSH-derived estimates [*Chelton et al.*, 2011]. These properties were then interpolated onto the Argo float surface fixes, and EKE was obtained by taking the difference between the YoMaHa velocity for each float cycle and the interpolated U_M. Equation (5) was then evaluated for all Argo data and averaged in the same bins as those used when estimating the observed diffusivities above. Standard deviations on the bin-averaged theoretical diffusivity were estimated by propagating the uncertainties in k, U_M, c, and EKE through equation (5).

Theoretical diffusivities and the suppression factor as a function of longitude are shown in Figure 9. The theoretical diffusivity varies less than the observed diffusivity and agrees with the lower values of the observed diffusivity. The largest mismatch is seen in regions where the observed diffusivity is elevated in comparison to background values. The suppression factor is always less than 1/2, implying that the diffusivity derived from standard mixing length arguments (K_0) is always suppressed in the presence of mean flow. It is interesting to note that the suppression factor suggests that there should be stronger suppression in regions where elevated diffusivity is observed and theoretical estimates show the greatest mismatch with the observed estimates of diffusivity. This is presumably because these are also the regions of elevated mean flow speed, as the ACC streamlines are squeezed together while traversing over the topographic features.

We conclude that theoretical estimates of *Ferrari and Nikurashin* [2010] and *Meredith et al.* [2011] capture the effect of mean flow that appears to be suppressing mixing within the Southern Ocean, as can be seen by the result that K_{eff} is reduced in comparison to K_0 and the suppression factor being less than 1/2. However, the assumptions used to reach equation (5) breakdown in the presence of topography, where the dynamics are more complicated than simple broad zonal jets with stochastic eddies.

5. Conclusion

We have demonstrated that within the Southern Ocean it is possible to obtain estimates of lateral diffusivity from Argo float trajectories. Numerical simulations in regions with significantly different flow structure and dynamics confirmed that the approach is robust. Regional tests with in situ Argo data in the South East Pacific Ocean/DIMES region produced estimates of diffusivities that are consistent with results from RAFOS floats and passive tracer that were released as part of DIMES [*Balwada et al.*, 2016; *LaCasce et al.*, 2014; *Tulloch et al.*, 2014].

We tested two different methods to obtain estimates of cross-stream diffusivity. In the first method we measure the displacement between a particle and the sea surface height contour on which it was deployed to

estimate cross-stream dispersion. In the second method we use two-particle dispersion in the uncorrelated limit and then calculate the eigenvalues to estimate the across and along mean flow diffusivities. To our knowledge, the second approach has not been used with observational data in any previous study. The two methods—single-particle and two-particle cross-stream diffusivities—were found to agree closely in the test cases considered with the two-particle method producing smaller error bars.

We applied these methods to Argo trajectories from the YoMaHa'07 data set to compute cross-stream diffusivities on a circumpolar basis in the Southern Ocean, averaged between 45°S and 65°S and at a depth of 1000 m. The cross-stream diffusivities varied between 300 and 2500 $m^2\ s^{-1}$, with regional variability dominated by peaks corresponding to five regions where the ACC interacts with topography: the Aghulas retroflection, the Kerguelen Plateau, the Campbell Plateau, part of the Pacific-Antarctic ridge, and the Scotia Sea. Comparison to previous studies demonstrated broad agreement within confidence intervals, where the differences are probably due to differences in geographical averaging between studies. Estimates of absolute meridional diffusivities ranged between 1000 and 10,000 $m^2\ s^{-1}$ and displayed similar regional variations to the cross-stream diffusivities. However, these meridional diffusivities did not match the estimates from cross-stream diffusivities because the ACC, which the dominant flow in the Southern Ocean, is not a simple broad zonal jet.

Finally, we compared our cross-stream diffusivities to predictions which incorporate suppression of mixing by the mean flow. A generally good agreement between the suppressed diffusivities and our estimates of cross-stream diffusivities was found, with the exception of regions of the Southern Ocean where the ACC interacts with topography. The theoretical estimates do a poor job at predicting the observed large variations that are set by the influence of topography on the mean flow.

Although local variations in deep eddy stirring associated with topography have been noted before, the explicit circumpolar quantification of eddy diffusivities across complex and smooth topography has not been clear. A further step will be to use these results to estimate parameterized eddy property transports across the ACC.

Appendix A: Does the Argo Cycle Induce Significant Diffusivity Errors? A Theoretical Perspective

The velocity of a Lagrangian particle can be written as

$$\frac{dX}{dt} = u. \tag{A1}$$

The velocity u can be separated in multiple components as $u = u_1H_1 + u_2H_2$ for Argo floats, where

$$H_1(t) = 1; x \in S \ = 0; x \in S'. \tag{A2}$$

For $S \cup S'$ is $t \in (-\infty, \infty)$.

We also define $H_2(t) = 1 - H_1(t)$. H_1 and H_2 are step functions to represent the behavior of an Argo float. H_1 is 1 when the float is at parking depth and 0 at all other times, whereas H_2 is 0 when float is at parking depth and 1 at all other times. Similarly, u_1 is the velocity at parking depth and u_2 is the velocity at all other depths during the float cycle. Using the definition of H_1 and H_2 we can also write $u(t) = u_1(t) + (u_2(t) - u_1(t))H_2(t)$.

The single-particle diffusivity is defined as [*LaCasce*, 2008; *Taylor*, 1921]

$$K(t) = \int_0^t u(X,t)u(X,\tau)d\tau. \tag{A3}$$

If we assume the turbulence to be spatially homogeneous then the X dependence in the velocities becomes irrelevant to the diffusivity, and

$$K(t) = \int_0^t u(t)u(\tau)d\tau.$$

Hence, we can split the velocity in the u_1 (velocity at parking depth) and u_2 (velocity away from parking depth) as a time series without worrying about how the Argo float might not have the same trajectory in

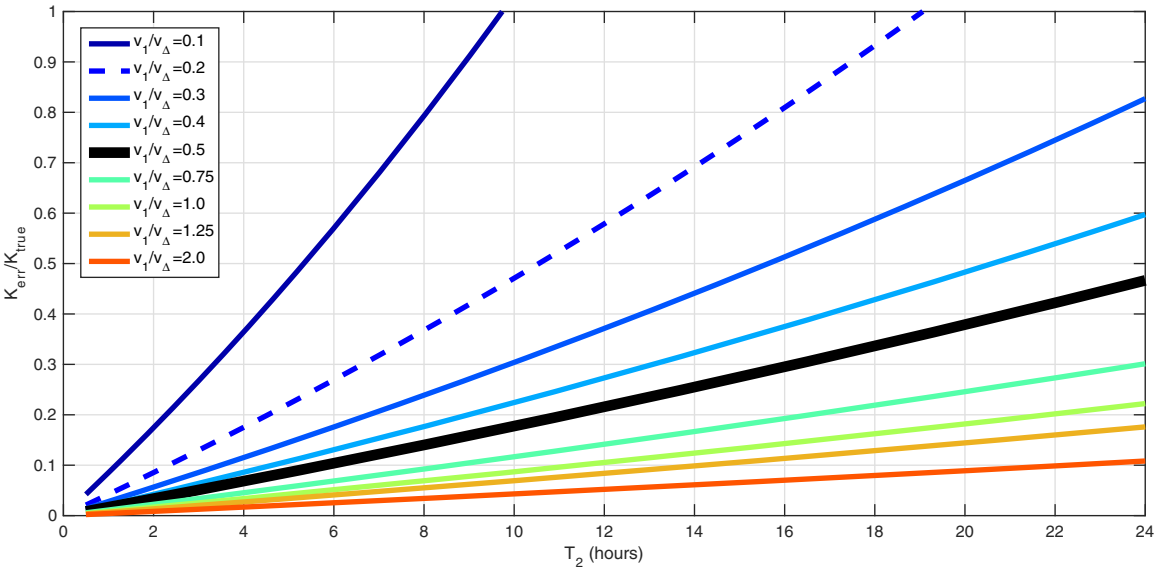


Figure A1. Ratio of K_{err} to K_{true} as a function of T_2 and v_1/v_Δ.

space as a particle following the path of a particle that is always at parking depth. Physically, one can envision this as saying that as the turbulent field is homogeneous in space and we are calculating a statistical measure of the fact that the exact float path may diverge from exact particle path is irrelevant as all paths measure the same turbulence.

Decomposing the velocity into components (where Δu denotes $u_2 - u_1$),

$$K(t) = \int_0^t u_1(t)u_1(\tau)d\tau + \int_0^t \Delta u(t)H_2(\tau)u_1(\tau)d\tau + \int_0^t u_1(t)\Delta u(\tau)H_2(\tau)d\tau + \int_0^t \Delta u(t)H_2(t)\Delta u(\tau)H_2(\tau)d\tau. \quad \text{(A4)}$$

We can write an autocovariance function as

$$\int_0^t u(t)u(\tau)d\tau = \upsilon^2 \int_0^t R(\tau)d\tau,$$

where $R(\tau)$ is the autocorrelation function for the velocities and v is the RMS velocity. If we assume that the process is stationary, the integral of the autocorrelation asymptotes to a Lagrangian time scale. We can, thus, rewrite the above equation in terms of time scales

$$K(t) = \upsilon_1{}^2 \int_0^t R_{11}d\tau + (\upsilon_\Delta.\upsilon_1)H_2(t)\int_0^t R_{\Delta 1}(\tau)d\tau + (\upsilon_\Delta.\upsilon_1)\int_0^t R_{\Delta 1}(\tau)H_2(\tau)d\tau + (\upsilon_\Delta.\upsilon_\Delta)H_2(t)\int_0^t R_{\Delta\Delta}(\tau)H_2(\tau)d\tau, \quad \text{(A5)}$$

where a subscript of 1 represents velocity scales of autocorrelation dependent on u_1 and a subscript of Δ those dependents on Δu.

The first term on the right-hand side is the diffusivity of a particle at the parking depth. We will call this term

$$K_{true} = \upsilon_1{}^2 T_{11},$$

where T_{11} is the Lagrangian time scale of particles at the parking depth.

The second term has an integral of an autocorrelation between the velocity at the parking depth and at other depths. We will assume the time scale associated with this integrated autocorrelation is the same as T_{11}. The integral in the third term is the same autocorrelation function as in the second term but now multiplied by a step function which is 0 over the parking period and 1 when away from the parking depth.

Assuming, conservatively, that the autocorrelation ($R1(\tau)$) decays slowly, the integral is the time spent away from the parking depth (T_2). Similarly a conservative estimate for the integral in the fourth term is also T_2.

Using the definition of diffusivity (equation (1)) at some suitably long time, greater than the time scales discussed above

$$\langle X^2\rangle(t)=2K_{true}t+2(\upsilon_\Delta.\upsilon_1)T_{11}\int_0^t H(t')dt'+2(\upsilon_\Delta.\upsilon_1)T_2t+2(\upsilon_\Delta.\upsilon_\Delta)T_2\int_0^t H_2(t')dt'. \tag{A6}$$

The integral asymptotes to ξt, where ξ is the ratio $T_2/(T_1 + T_2)$. T_1 is the time spent at the parking depth and T_2 is the time spent away from the parking depth.

$$\langle X^2\rangle(t)=2K_{true}t+2K_{err}t, \tag{A7}$$

where

$$K_{err}=(\upsilon_\Delta.\upsilon_1)T_{11}\xi+(\upsilon_\Delta.\upsilon_1)T_2t+(\upsilon_\Delta.\upsilon_\Delta)T_2\xi. \tag{A8}$$

The circumpolar RMS deep currents speed is 0.049 m s^{-1}, with a corresponding surface RMS speed of 0.160 m s^{-1}, giving $v_1 \sim 0.05$ m s^{-1} and $v_\Delta \sim 0.1$ m s^{-1}. We will assume the Lagrangian time scale T_{11} is 10 days.

Choosing T_2 is a more difficult matter, while above we have defined it as the time spent away from parking depth we have also assumed during that time the float is exposed to the full surface velocity. Selection of a representative figure is thus dependent upon the vertical structure of the flow: if we assume geostrophic flow is purely barotropic with the v_Δ derived solely from Ekman currents an appropriate T_2 will be effectively equal to the time spent on the surface; conversely, if geostrophic shear is strong across the entire water column, then T_2 will be longer than the time spent at the surface. For ARGOS-equipped floats this gives a range on T_2 of 9–18 h, with the upper limit corresponding to the float experiencing v_Δ from the time it passes the parking depth during the upward profile to the time it returns to the parking depth on descent. For Iridium-equipped floats the corresponding range is be 1–8 h.

In light of this we plotted the ratio K_{err}/K_{true} for T_2 ranging between 0.5 and 24 h (Figure A1, black line) assuming a 10 day float cycle. Errors increased from 20% at $T_2 = 12$ h to 34% at $T_2 = 18$ h. We also examined the effect of varying the ratio between v_1 and v_Δ (shown here for a v_Δ of 0.1 m s^{-1}, but similar behavior applies for other v_Δ). As shown in Figure A1, larger deep velocities (green to red lines lines) corresponded with reduced errors. Smaller deep velocities (blue lines) saw significantly increased errors, with, for example, a 60% error at $T_2 = 18$ h for $v_1/v_\Delta = 0.3$. By way of comparison, errors on single-particle cross-contour diffusivities presented above typically range between 30 and 50% of the mean value, with previous studies producing similar or larger errors.

The above analysis indicates that even taking relatively pessimistic assumptions, within the range of parameters seen in a large-scale view of the ocean, errors in single-particle diffusivity induced by Argo float profiling behavior are less than or comparable to errors induced by inhomogenieties in the ocean; the eddy processes being of nondiffusive nature and lack of sufficient float data; errors that are omnipresent in any observational study of diffusivity. Thus, we conclude in the large-scale Southern Ocean context Argo float trajectories can provide a suitable alternative to RAFOS floats or chemical tracers.

Examination of 1° × 1° maps of v_1/v_Δ from the YoMaHa '07 data set (not shown) indicate for the vast majority of the Southern Ocean and most western boundary currents, v_1/v_Δ exceeds 0.3, thus are likely to produce acceptable errors when computing diffusivities from ARGOS-tracked Argo float trajectories. The interior of the major ocean gyres produce smaller values of v_1/v_Δ, suggesting ARGOS-tracked floats will not produce usable diffusivities in these regions. However, the increasing use of Iridium-tracked floats, with associated shorter surface drift periods and lower profiling-induced errors, should allow finer-scale robust estimates of eddy diffusivities in the interior of ocean gyres possible within the next few years.

Acknowledgments
We wish to thank Catherine Hancock for processing the DIMES RAFOS float data. We acknowledge the assistance of Erik Van Sebille in resolving a number of issues with the Connectivity Modelling System particle tracking package. We wish to thank the two anonymous reviewers for a number of suggestions which helped improve this paper. Funding for this research was provided by NSF OCE 1231803, NSF OCE 0622670, and NSF OCE 0822075. For access to the cross-stream diffusivity estimates contact Christopher Roach (croach@hawaii.edu). For access to the DIMES RAFOS float data contact Catherine Hancock (chancock@fsu.edu). Monthly updates of the YoMaHa'07 data set are available from http://apdrc.soest.hawaii.edu/projects/yomaha/. The Southern Ocean State Estimate data set can be accessed at http://sose.ucsd.edu/sose_stateestimation_data_05to10.html. Mean Dynamic Topography is sourced from AVISO at http://www.aviso.altimetry.fr. The Connectivity Modelling System particle tracking package is available at https://github.com/beatrixparis/connectivity-modeling-system.

References

Balwada, D., K. G. Speer, J. H. LaCasce, W. B. Owens, J. Marshall, and R. Ferrari (2016), Circulation and Stirring in the Southeast Pacific Ocean and the Scotia Sea Sectors of the Antarctic Circumpolar Current, *J. Phys. Oceanogr.*

Bolster, D., M. Dentz, and T. Le Borgne (2011), Hypermixing in linear shear flow, *Water Resour. Res.*, *47*, W09602, doi:10.1029/2011WR010737.

Chelton, D. B., M. G. Schlax, and R. M. Samelson (2011), Global observations of nonlinear mesoscale eddies, *Prog. Oceanogr.*, *91*(2), 167–216, doi:10.1016/j.pocean.2011.01.002.

Chiswell, S. M. (2013), Lagrangian time scales and eddy diffusivity at 1000 m compared to the surface in the South Pacific and Indian Oceans, *J. Phys. Oceanogr.*, *43*(12), 2718–2732, doi:10.1175/JPO-D-13-044.1.

Cole, S. T., C. Wortham, E. Kunze, and W. B. Owens (2015), Eddy stirring and horizontal diffusivity from Argo float observations: Geographic and depth variability, *Geophys. Res. Lett.*, *42*, 3989–3997, doi:10.1002/2015GL063827.

Davis, R. E. (1991a), Lagrangian ocean studies, *Annu. Rev. Fluid Mech.*, *23*(1), 43–64.

Davis, R. E. (1991b), Observing the general circulation with floats, *Deep Sea Res., Part A*, *38*, S531–S571.

Deng, Z., T. Yu, S. Shi, J. Jin, and K. Wu (2014), The global distribution of diapycnal mixing and mixing coefficient tensor in the upper 2000 m ocean from Argo observations, *Mar. Geod.*, *37*(3), 337–353.

Faure, V., and K. Speer (2012), Deep circulation in the eastern South Pacific Ocean, *J. Mar. Res.*, *70*(5), 748–778.

Ferrari, R., and M. Nikurashin (2010), Suppression of eddy diffusivity across jets in the Southern Ocean, *J. Phys. Oceanogr.*, *40*(7), 1501–1519.

Griesel, A., S. T. Gille, J. Sprintall, J. L. McClean, J. H. LaCasce, and M. E. Maltrud (2010), Isopycnal diffusivities in the Antarctic Circumpolar Current inferred from Lagrangian floats in an eddying model, *J. Geophys. Res.*, *115*, C06006, doi:10.1029/2009JC005821.

Griesel, A., J. L. McClean, S. T. Gille, J. Sprintall, and C. Eden (2013), Eulerian and Lagrangian isopycnal eddy diffusivities in the Southern Ocean of an eddying model, *J. Phys. Oceanogr.*, *44*(2), 644–661, doi:10.1175/JPO-D-13-039.1.

Katsumata, K., and H. Yoshinari (2010), Uncertainties in global mapping of Argo drift data at the parking level, *J. Oceanogr.*, *66*(4), 553–569, doi:10.1007/s10872-010-0046-4.

Klocker, A., R. Ferrari, and J. H. LaCasce (2012a), Estimating suppression of eddy mixing by mean flows, *J. Phys. Oceanogr.*, *42*(9), 1566–1576, doi:10.1175/JPO-D-11-0205.1.

Klocker, A., R. Ferrari, J. H. LaCasce, and S. T. Merrifield (2012b), Reconciling float-based and tracer-based estimates of eddy, *J. Mar. Res.*, *70*, 569–602.

LaCasce, J. H. (2008), Statistics from Lagrangian observations, *Prog. Oceanogr.*, *77*(1), 1–29.

LaCasce, J. H., and C. Ohlmann (2003), Relative dispersion at the surface of the Gulf of Mexico, *J. Mar. Res.*, *61*(3), 285–312.

LaCasce, J. H., R. Ferrari, J. Marshall, R. Tulloch, D. Balwada, and K. Speer (2014), Float-derived isopycnal diffusivities in the DIMES experiment, *J. Phys. Oceanogr.*, *44*(2), 764–780, doi:10.1175/JPO-D-13-0175.1.

Lagerloef, G. S., G. T. Mitchum, R. B. Lukas, and P. P. Niiler (1999), Tropical Pacific near-surface currents estimated from altimeter, wind, and drifter data, *J. Geophys. Res.*, *104*(C10), 23,313–23,326.

Lebedev, K. V., H. Yoshinari, N. A. Maximenko, and P. W. Hacker (2007), Velocity data assessed from trajectories of Argo floats at parking level and at the sea surface, *IPRC Tech. Note*, *4*(2), 1–16.

Marshall, J., and K. Speer (2012), Closure of the meridional overturning circulation through Southern Ocean upwelling, *Nat. Geosci.*, *5*(3), 171–180.

Massey, F. J. (1951), The Kolmogorov-Smirnov test for goodness of fit, *J. Am. Stat. Assoc.*, *46*(253), 11–121.

Mazloff, M. R., P. Heimbach, and C. Wunsch (2010), An eddy-permitting southern ocean state estimate, *J. Phys. Oceanogr.*, *40*(5), 880–899, doi:10.1175/2009JPO4236.1.

Meredith, M. P., A. C. Naveira Garabato, A. M. Hogg, and R. Farneti (2011), Sensitivity of the overturning circulation in the Southern Ocean to decadal changes in wind forcing, *J. Clim.*, *25*(1), 99–110, doi:10.1175/2011JCLI4204.1.

Naveira-Garabato, A. C., D. P. Stevens, A. J. Watson, and W. Roether (2007), Short-circuiting of the overturning circulation in the Antarctic Circumpolar Current, *Nature*, *447*(7141), 194–197.

Ollitrault, M., and J.-P. Rannou (2012), ANDRO: An Argo-based deep displacement dataset, *J. Atmos. Oceanic Technol.*, *30*(4), 759–788, doi:10.1175/JTECH-D-12-00073.1.

Paris, C. B., J. Helgers, E. van Sebille, and A. Srinivasan (2013), Connectivity Modeling System: A probabilistic modeling tool for the multi-scale tracking of biotic and abiotic variability in the ocean, *Environ. Modell. Software*, *42*, 47–54, doi:10.1016/j.envsoft.2012.12.006.

Phillips, H. E., and S. R. Rintoul (2000), Eddy variability and energetics from direct current measurements in the Antarctic Circumpolar Current south of Australia, *J. Phys. Oceanogr.*, *30*, 3050–3076.

Rio, M. H., and F. Hernandez (2004), A mean dynamic topography computed over the world ocean from altimetry, in situ measurements, and a geoid model, *J. Geophys. Res.*, *109*, C12032, doi:10.1029/2003JC002226.

Rohatgi, V. K., and A. K. M. Ehsanes Saleh (1976), *An Introduction to Probability and Statistics*, 2nd ed., John Wiley, N. Y.

Rypina, I., M. Brown, F. Beron-Vera, H. Koçak, M. Olascoaga, and I. Udovydchenkov (2007), Robust transport barriers resulting from strong Kolmogorov-Arnold-Moser stability, *Phys. Rev. Lett.*, *98*(10), 104102.

Sallee, J.-B., K. Speer, and S. Rintoul (2011), Mean-flow and topographic control on surface eddy-mixing in the Southern Ocean, *J. Mar. Res.*, *69(4–6)*, 753–777.

Speer, K., S. R. Rintoul, and B. Sloyan (2000), The diabatic deacon cell, *J. Phys. Oceanogr.*, *30*, 3212–3222.

Swenson, M. S., and P. P. Niiler (1996), Statistical analysis of the surface circulation of the California Current, *J. Geophys. Res.*, *101*, 22,631–622,645.

Taylor, G. (1921), Diffusion by continuous movements, *Proc. London Math. Soc.*, *20*, 196–211.

Tulloch, R., R. Ferrari, O. Jahn, A. Klocker, J. LaCasce, J. R. Ledwell, J. Marshall, M.-J. Messias, K. Speer, and A. Watson (2014), Direct estimate of lateral eddy diffusivity upstream of drake passage, *J. Phys. Oceanogr.*, *44*(10), 2593–2616, doi:10.1175/JPO-D-13-0120.1.

Zhurbas, V., and I. S. Oh (2003), Lateral diffusivity and Lagrangian scales in the Pacific Ocean as derived from drifter data, *J. Geophys. Res.*, *108*(C5), 3141, doi:10.1029/2002JC001596.

Zhurbas, V., and I. S. Oh (2004), Drifter - derived maps of lateral diffusivity in the Pacific and Atlantic oceans in relation to surface circulation patterns, *J. Geophys. Res. Oceans*, *109*(C5).